S. Department
Transportation
ederal Railroad
dministration

Finite Element Models, Validation, and Results for Wheel Temperature and Elastic Thermal Stress Distributions

ffice of Research
id Development
ashington, DC 20590

Y. H. Tang
J. E. Gordon
A. B. Perlman
O. Orringer

Research and
Special Programs
Administration
John A. Volpe National
Transportation Systems Center
Cambridge, MA 02142-1093

OT/FRA/ORD-93/17
OT-VNTSC-FRA-93-21

Final Report
September 1993

NOTICE

This document is disseminated under the sponsorship of the Department of Transportation in the interest of information exchange. The United States Government assumes no liability for its contents or use thereof.

NOTICE

The United States Government does not endorse products or manufacturers. Trade or manufacturers' names appear herein solely because they are considered essential to the object of this report.

REPORT DOCUMENTATION PAGE

Form Approved
OMB No. 0704-0188

1. AGENCY USE ONLY (Leave blank)	2. REPORT DATE	3. REPORT TYPE AND DATES COVERED
	September 1993	Final Report November 1992 - February 1993

4. TITLE AND SUBTITLE
Finite Element Models, Validation, and Results for Wheel Temperature and Elastic Thermal Stress Distributions

5. FUNDING NUMBERS
R3026/RR328

6. AUTHOR(S)
Y.H. Tang, J.E. Gordon, A.B. Perlman and O. Orringer

7. PERFORMING ORGANIZATION NAME(S) AND ADDRESS(ES)
U.S. Department of Transportation
Research and Special Programs Administration
John A. Volpe National Transportation Systems Center
Cambridge, MA 02142

8. PERFORMING ORGANIZATION REPORT NUMBER
DOT-VNTSC-FRA-93-21

9. SPONSORING/MONITORING AGENCY NAME(S) AND ADDRESS(ES)
Federal Railroad Administration
Office of Research and Development
Washington, DC 20590

10. SPONSORING/MONITORING AGENCY REPORT NUMBER
DOT/FRA/ORD-93/17

11. SUPPLEMENTARY NOTES

12a. DISTRIBUTION/AVAILABILITY STATEMENT
This document is available to the public through the National Technical Information Service, Springfield, VA 22161

12b. DISTRIBUTION CODE

13. ABSTRACT (Maximum 200 words)

This report is the third in a series of engineering studies on railroad vehicle wheel performance. Heat transfer finite element models of multiple unit (MU) power car wheels are documented and validated by comparison of calculated temperatures with measurements made during an operational test. Elastic finite element stress models are used to compare thermal stress effects in wheels having two different plate designs. As compared with the stiff straight plate, flexible "S" plate is found to reduce the calculated stress magnitude by 30% to 50% under drag braking conditions. However, the stress reduction is found to be only 10% under typical MU stop braking conditions.

14. SUBJECT TERMS
Thermal Stress; Wheels

15. NUMBER OF PAGES
46

16. PRICE CODE

17. SECURITY CLASSIFICATION OF REPORT	18. SECURITY CLASSIFICATION OF THIS PAGE	19. SECURITY CLASSIFICATION OF ABSTRACT	20. LIMITATION OF ABSTRACT
Unclassified	Unclassified	Unclassified	

PREFACE

This report is the third of a series of engineering studies on railroad vehicle wheel performance. Preliminary studies involving evaluation of actions taken to respond to high rates of crack occurrence observed in the wheels of certain multiple unit (MU) power cars used in commuter service, were summarized in the first report. The second report documented an operational test which was conducted to determine the effects of high-performance stop braking on temperature distributions in the MU wheels. In this report, heat transfer and stress finite models of the MU wheels are documented. The heat transfer models are validated by comparison of calculated temperature distributions with temperature measurements from the operational test.

METRIC/ENGLISH CONVERSION FACTORS

ENGLISH TO METRIC

LENGTH (APPROXIMATE)

1 inch (in) = 2.5 centimeters (cm)
1 foot (ft) = 30 centimeters (cm)
1 yard (yd) = 0.9 meter (m)
1 mile (mi) = 1.6 kilometers (km)

AREA (APPROXIMATE)

1 square inch (sq in, in^2) = 6.5 square centimeters (cm^2)
1 square foot (sq ft, ft^2 = 0.09 square meter (m_2)
1 square yard (sq yd, yd^2) = 0.8 square meter (m^2)
1 square mile (sq mi, mi^2) = 2.6 square kilometers (km^2)
1 acre = 0.4 hectares (he) = 4,000 square meters (m^2)

MASS - WEIGHT (APPROXIMATE)

1 ounce (oz) = 28 grams (gr)
1 pound (lb) = .45 kilogram (kg)
1 short ton = 2,000 pounds (lb) = 0.9 tonne (t)

VOLUME (APPROXIMATE)

1 teaspoon (tsp) = 5 milliliters (ml)
1 tablespoon (tbsp) = 15 milliliters (ml)
1 fluid ounce (fl oz) = 30 milliliters (ml)
1 cup (c) = 0.24 liter (1)
1 pint (pt) = 0.47 liter (1)
1 quart (qt) = 0.96 liter (1)
1 gallon (gal) = 3.8 liters (1)
1 cubic foot (cu ft, ft^3) = 0.03 cubic meter (m^3)
1 cubic yard (cu yd, yd^3) = 0.76 cubic meter (m^3)

TEMPERATURE (EXACT)

[(x-32)(5/9)] ^oF = y ^oC

METRIC TO ENGLISH

LENGTH (APPROXIMATE)

1 millimeter (mm) = 0.04 inch (in)
1 centimeter (cm) = 0.4 inch (in)
1 meter (m) = 3.3 feet (ft)
1 meter (m) = 1.1 yards (yd)
1 kilometer (km) = 0.6 mile (mi)

AREA (APPROXIMATE)

1 square centimeter (cm^2) = 0.16 square inch (sq in, in^2)
1 square meter (m^2) = 1.2 square yeards (sq yd, yd^2)
1 square kilometer (km^2) = 0.4 square mile (sq mi, mi^2)
1 hectare (he) = 10,000 square meters (m^2) = 2.5 acres

MASS - WEIGHT (APPROXIMATE)

1 gram (gr) = 0.036 ounce (oz)
1 kilogram (kg) = 2.2 pounds (lb)
1 tonne (t) = 1,000 kilograms (kg) = 1.1 short tons

VOLUME (APPROXIMATE)

1 milliliters (ml) = 0.03 fluid ounce (fl oz)
1 liter (1) = 2.1 pints (pt)
1 liter (1) = 1.06 quarts (qt)
1 liter (1) = 0.26 gallon (gal)
1 cubic meter (m^3) = 36 cubic feet (cu ft, ft^3)
1 cubic meter (m^3) = 1.3 cubic yards (cu yd, yd^3)

TEMPERATURE (EXACT)

[(9/5) y + 32] ^oC = x ^oF

QUICK INCH-CENTIMETER LENGTH CONVERSION

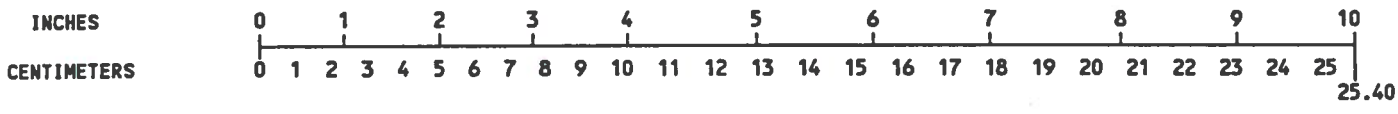

QUICK FAHRENHEIT-CELSIUS TEMPERATURE CONVERSION

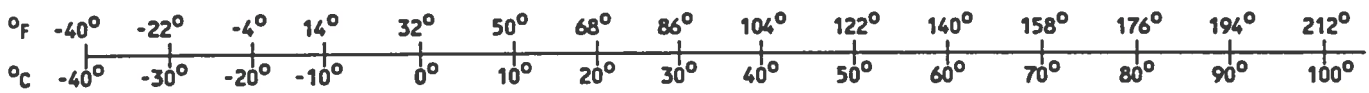

For more exact and or other conversion factors, see NBS Miscellaneous Publication 286, Units of Weights and Measures. Price $2.50. SD Catalog No. C13 10286.

TABLE OF CONTENTS

LIST OF ILLUSTRATIONS

LIST OF ILLUSTRATIONS (cont'd)

LIST OF TABLES

1. INTRODUCTION

This report is the third of a series on the results of an engineering study of the effects of service loads on railroad vehicle wheels. The study was initiated in September 1991, in response to a request for assessment of contributing factors and corrective actions taken regarding high rates of crack occurrence in certain multiple unit (MU) powered cars used in commuter service. The ultimate goal of the study is the evaluation of safe limits on performance demand (weight carried per wheel, maximum speed, vehicle braking rate) as a function of wheel design, material selection, and manufacture, as well as percentage of braking effort absorbed through the wheel tread in service. The models developed in the study are intended to provide the capability for similar engineering design analyses of other railroad vehicle wheels besides the types used on MU cars.

1.1 Background

Special inspections of commuter rail vehicles conducted by the Federal Railroad Administration (FRA) Office of Safety in 1991 revealed chronic problems of cracking in the wheels of powered MU cars operated by three railroads serving the Greater New York area. The car design types are similar, but the vehicle characteristics and wheel cracking features were found to have significant differences.

The highest rate of cracking was found in the wheels of moderate weight vehicles, operated at moderate speeds, and equipped with blended dynamic braking to supplement the wheel tread brakes. The wheel cracks in this fleet, predominantly of thermal origin at the front rim edge, were attributed to maintenance problems: (1) dispatching of vehicles with inoperative traction motors, and thus also inoperative dynamic braking; and (2) inadequate tread brake unit refurbishment, leading to brake shoes riding over the front rim edge.

A comparable rate of cracking was found in the wheels of moderate weight vehicles, operated at high speed (100 mph), and equipped solely with tread brakes. The wheel cracks in this fleet, of thermal origin in the center tread position, were attributed to the demand for heat absorption through the tread imposed by high-speed operation without auxiliary brakes.

A lower rate of cracking with mixed thermal and mechanical origins was found in the third fleet. This fleet consists of heavy vehicles, operated at moderate speeds, and equipped with blended dynamic braking to supplement the tread brakes. The combination of vehicle weight, heat input to the wheel tread, and occasional maintenance problems were identified as the factors contributing to wheel cracks in this case.

The FRA Office of Safety took immediate actions to assure continuing operational safety as soon as evidence of chronic wheel cracking was revealed. These actions included specific requirements to address identified maintenance problems and general requirements for daily inspection of wheels in service. Wheels found to have cracks must be shopped and re-trued to remove all crack indications before being returned to service. The general requirements prudently established a safety first policy, under the circumstances of frequent crack occurrence but lack of accurate critical[1] crack size information. Since compliance places

---

1 "Critical" as used here means a crack just large enough to precipitate wheel fracture under existing service conditions.

economic burdens on the affected railroads, the Office of Safety requested an engineering study to: (1) evaluate the effectiveness of the immediate actions; and (2) develop rational options for long-term solutions.

Each affected railroad also started to take longer term actions and develop options for lasting solutions. Actions already taken include upgrade of material properties and adoption of an advanced plate design in the specifications for new wheel orders and, for those MU cars not so equipped, retrofit of new motors with dynamic braking capability. Options under development include route studies to identify segments where speed reductions might provide effective relief without undue schedule penalty, further advancement of wheel design, and improvement of brake shoe material and/or design.

1.2 Preliminary Engineering Studies

Several preliminary study tasks were undertaken from September 1991 through September 1992. Initially, the wheel maintenance records of the affected railroads were reviewed to confirm the general nature of the crack occurrence patterns.[2] The frequency of re-trueing in some cases suggested that wheels were developing visible thermal cracks in weeks. Wheel service life in such cases appeared to be limited by the re-trueing necessary to remove crack indications.

Two wheels removed from service for center tread thermal cracks were destructively tested to obtain quantitative data on the number and size of the cracks [1].[3] Each tread surface was first surveyed with the aid of fluorescent magnetic particle inspection to locate the cracks and measure their visible lengths. Each wheel was then mounted on a vertical boring mill and re-faced in short steps from the front rim face toward the flange to permit determination of the crack depths.[4] The test wheels were found to have, respectively, 69 and 160 identifiable center tread thermal cracks with visible lengths ranging from 0.5 inch (13 mm)[5] to 1.15 inches (29 mm), with no crack depth exceeding 0.33 inch (8.4 mm). The other significant findings were that all cracks were visible on the tread surface, and that the visible length of each crack was also its maximum length.

A new wheel and the mate to one of the above wheels were also subjected to destructive saw cutting to provide displacement data for estimation of residual stresses in the rim.[6] The procedure for measuring the displaced cut profile was improved by means of moire instrumentation [2], but the method used to estimate the residual stresses from the displacement data was the same as that developed by the Association of American Railroads for an earlier program of research on freight car wheels [3]. The analysis of test results

---

2 Inquiries were also made through other FRA region offices to determine whether other railroads were experiencing similar problems (no comparable occurrence rates were found).

3 References are listed on page 23.

4 Shop support was provided by the ORX Railway Corporation, Tipton, PA.

5 Center tread thermal cracks do not become visually identifiable as such until the visible length reaches about 1/2 inch.

6 Shop support was provided by the Norfolk Southern Railroad Research Laboratory, Alexandria, VA.

indicated outer rim hoop stresses about 42 ksi (290 MPa) compression in the new wheel but only 20 ksi (140 MPa) compression in the used wheel. The retention of some compression in a used wheel was encouraging, since compressive stress tends to close and delay the growth of cracks. However, the saw cut tests did not provide the data necessary to reliably determine the depth below tread at which a crack would encounter tensile hoop stress.

Metallographic examination and hardness testing [4] of sections taken from the mate wheel established depth below tread limits for the following phenomena: (1) heavily deformed plastic zone indicated by sheared elongated grain shape to a depth of 0.0008 inch (0.02 mm); (2) heat affected zone indicated by presence of spherodized microstructure to a depth of 0.02 inch (0.5 mm); and (3) layer work-hardened to an approximate average of RC 43 to a depth of 0.02 inch (0.5 mm).[7] Fractographic examination of fatigue crack growth surfaces confirmed the tendency of the cracks to grow much more slowly in depth as the maximum depth approached 0.2 to 0.3 inch (5 to 8 mm), but lateral growth toward the flange and front rim face appeared to continue unabated. Conversely, fractographic examination of another center tread crack in a wheel that had also been subjected to drag braking showed evidence of rapid propagation (fracture and arrest) events, beginning when the crack was about 1/2 inch long on the tread surface.

Laboratory specimens from the new wheel were also subjected to combined high temperature and rapid plastic compression, followed by air cooling, to simulate the combination of stop-braking and wheel/rail contact effects [5]. Metallographic examination [6] revealed a spherodized microstructure, similar to that observed near the used wheel tread, in those specimens which had been subjected to at least 5% compressive strain and temperatures in the pearlite - austenite transformation range, 1340 to 1430 ^{o}F (727 to 777 ^{o}C).

Heat transfer calculations with a preliminary model also suggested that wheel tread temperatures up to 1300 ^{o}F (704 ^{o}C) could be attained as a result of the high-performance stop-braking profiles experienced by the MU cars. More detailed calculations with a finite element model showed that an overhanging brake shoe could produce temperatures in the transformation range near the front rim edge, under otherwise normal operating conditions.

The picture which emerged from the preliminary studies suggested that cracks of thermal origin are the main concern, and that a process of shallow stress reversal is responsible for the formation of such cracks in the wheels of the MU cars. Stress reversal (from hoop compression to tension) is a well known cause of thermal cracking and fracture in freight car wheels which have been subjected to repeated drag braking for long time intervals at low power, but in such cases the stress is usually reversed in the bulk of the rim, most of which is heated to high temperature. Conversely, typical stop-braking profiles involve high power for short time intervals and tend to flash-heat the outer rim region to temperatures much higher than those in the bulk of the rim. The thermal stresses, which are induced by temperature gradients, then concentrate in the outer rim region. Thus, wheel thermal response to stop braking is not necessarily indicated by its response to drag braking. Also, any subsequent drag braking can apparently cause rapid propagation of thermal cracks which have formed under less severe conditions.

---

7 The base material has a pearlitic microstructure with approximate hardness RC 35 below the heat affected and work-hardened zones.

Based on these findings, the decision was made to develop a set of detailed finite element models which could be used to evaluate the potential for different types of wheels to resist cracking under various combinations of service conditions. The approach, relation between models, and relation of models to validation tests are outlined in the following section.

1.3 Overview of Detailed Engineering Studies

The wheels of a typical MU car experience on the order of 10^4 stop braking events and 10^7 wheel/rail contact cycles[8] in a year of service. Many stops and contact cycles are thus involved, even if rim stress is reversed in just a few days or weeks. The performance demand (weight carried per wheel, maximum speed, vehicle braking rate) may either modify or reverse the residual hoop stress in the rim. These outcomes can be distinguished by assuming that the modified or reversed stresses are stable, i.e., they are not changed simply by further repetition of the same performance demands after some period of service has elapsed. Such states, referred to as shakedown stresses, can be calculated from the known initial conditions (residual stress from manufacture) and descriptions of the loads imposed by repeated performance demands.

A recently developed method for estimating shakedown stresses in a body requires only that each load be described in terms of the stress magnitudes it would cause in the body, assuming purely elastic behavior [7]. This task is easily accomplished by means of elastic finite element stress analysis models. The method has been successfully applied to the problem of estimating shakedown stresses in rails [8], including cases in which initial conditions must be accounted for [9,10]. This method can also be used to estimate wheel shakedown stresses, with both mechanical (weight per wheel) and thermal (braking) loads as inputs.

The block diagram in Figure 1 illustrates the organization of models and tests required to develop a realistic procedure for estimating wheel shakedown stresses. The shaded blocks denote items covered in this report. The dashed box encloses those items which constitute the inputs and output of the wheel shakedown stress model.

The other blocks in Figure 1 represent the tasks required to prepare the inputs for the shakedown stress model. The theoretical paths are emphasized because the models can produce complete descriptions of input stresses which also conform to the laws of mechanical equilibrium. Completeness and conformity are necessary to avoid propagation and amplification of numerical errors in the shakedown stress calculations. Conversely, experimental stress analyses usually cover only part of the body, and the results often contain equilibrium errors when measurements are made on complex bodies such as wheels or rails [3,8]. In spite of these limitations, experiments are still essential for checking the realism of the models.

The most challenging tasks are those required for estimation of initial manufacturing stresses. The saw cut test and data analysis provide only a partial indication of the residual stresses in a wheel. Accurate information can be obtained about the distribution of hoop stress in the outer rim, where the cut has passed through, because the hoop component is fully relieved at the cut surface. The other stress components are only partially relieved at the cut,

---

8 "Cycle" refers to the repetition of contact stresses, at a typical point in the rim, in each wheel revolution.

and only minor relief occurs at locations beyond the cut. However, the measured outer rim hoop stress provides a good check on the order of magnitude of the residual stresses calculated from the models.

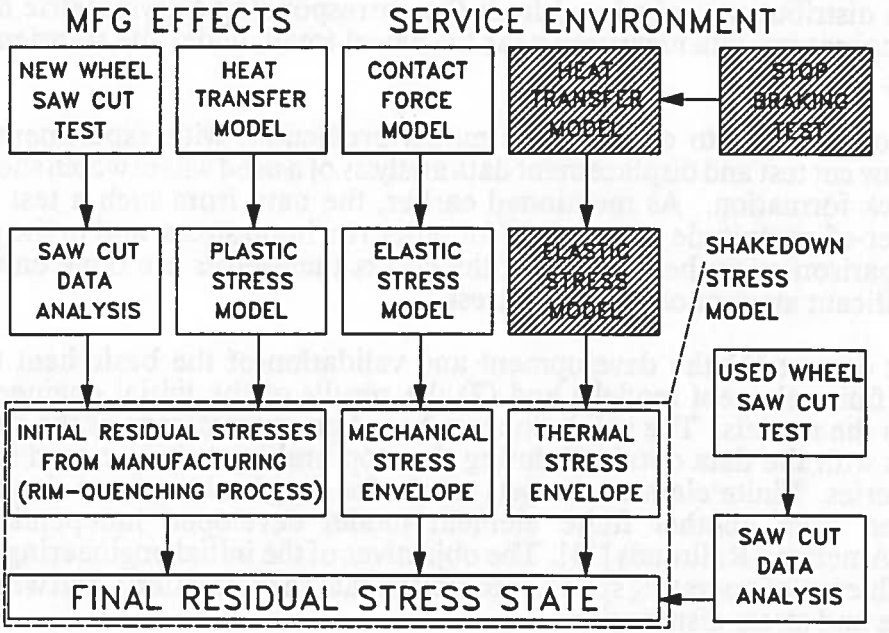

Figure 1. Model and Test Relationships.

Two-dimensional heat transfer and elastic-plastic stress finite element models can be used to estimate the manufacturing stresses, under the reasonable assumption that the heat treatment process is axially symmetric. The heat and stress analyses are done independently, but each requires further assumptions about physical parameters and high-temperature material properties. The model parameters must be adjusted until the calculated outer rim hoop stress is in reasonable agreement with the saw cut data analysis results.

Wheel/rail contact is generally modeled by means of semi-analytical techniques based on influence functions. The influence function is a description of displacements or stresses, in either body, caused by a concentrated force of unit magnitude applied to the body's surface. The theory of contact mechanics is mainly concerned with the application of displacement influence functions to calculate the area of contact, together with distributions of pressure and shear on the contact area, under various assumptions about the behavior of the contacting bodies [11]. For engineering design or detailed stress analysis, the contact model is often simplified by treating the bodies as elastic media and applying the basic Hertz contact theory. Calculations of this type have been used to provide the imposed stress input to incremental elastic-plastic finite element analyses of wheels [12,13]. A similar approach is taken in the present case, but with the added advantage that the elastic contact analysis is consistent with the assumptions of the shakedown theory. The numerical analysis must be three-dimensional, however, including a three-dimensional finite element model to account for the gross load stresses, even though the shakedown analysis itself is ultimately two-dimensional in character.

Thermal stress analysis requires only a two-dimensional finite model, under the reasonable assumption that the wheel revolves rapidly enough to distribute the braking energy axisymmetrically. Elastic material behavior may be assumed, in accordance with the shakedown model input requirements. The essential validation requirement is comparison of temperature distributions calculated from the corresponding axisymmetric heat transfer model with temperature data measured near the wheel tread, under the transient conditions of stop braking.

One more opportunity to compare the model predictions with experimental results is provided by a saw cut test and displacement data analysis of a used wheel which shows evidence of thermal crack formation. As mentioned earlier, the data from such a test can at most provide an order-of-magnitude comparison for outer rim hoop stress, and in the present case even that comparison might be distorted if the cracks themselves are large enough to have relieved a significant amount of the hoop stress.

This report covers: (1) the development and validation of the basic heat transfer and thermal stress finite element models; and (2) the results of the initial engineering studies conducted with the models. The validation was based on comparisons of the finite element analysis results with the data obtained during the stop braking test discussed in the second report in this series. Finite element analysis results for drag braking were also compared to results obtained from another finite element model developed independently by the Association of American Railroads [14]. The objectives of the initial engineering studies were to assess the influence of operating speed, retardation rate (deceleration), and wheel geometry on temperature and stress distributions.

2. MODELING

Finite element programs obtained from the Lawrence Livermore National Laboratory were used to perform thermal [15] and elastic stress [16] analyses on straight plate and S-plate wheels. To construct a simulation using finite element analysis, the geometry of the model is represented by a mesh of elements. For the heat transfer analysis (TOPAZ), heat flow at the tread is a boundary condition. The temperature state data from TOPAZ is used as the loading condition for the stress analysis (NIKE).

2.1 Geometry

The wheel geometry was modeled in three sections (rim, plate and hub), as shown in Figure 2. Heat penetrates the tread surface of the wheel during brake application. The depth of heat penetration into the wheel depends on the magnitude and duration of heat flow at the tread surface. The maximum temperature increases as the duration of heat flow increases.

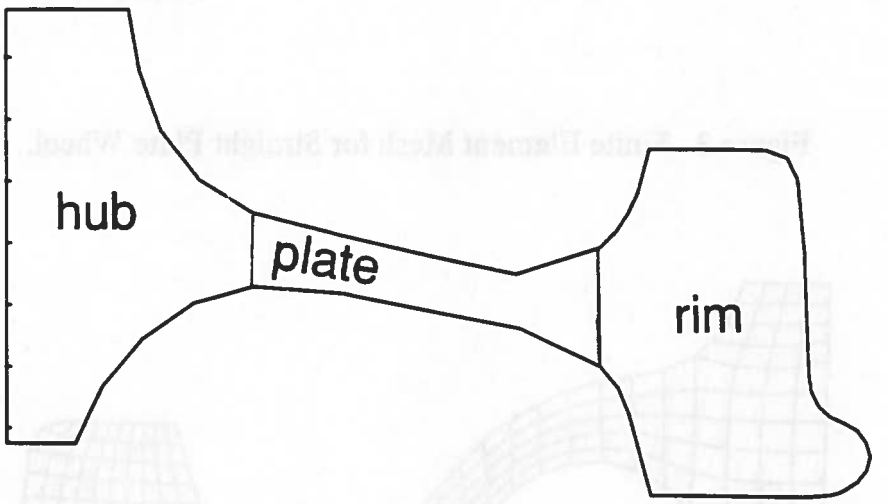

Figure 2. Wheel Subregions for Finite Element Model.

Since the representation of temperature and stress gradients depends on the mesh in the rim area, it is necessary to model the rim area with good accuracy. During operation, the wheel is assumed to rotate at a relatively high speed, such that the heat is distributed uniformly around the circumference. Therefore, only the cross section of the wheel is required to generate an axisymmetric model. Profiles of 32-inch diameter straight plate and S-plate wheels were digitized and converted into finite element meshes using a 2D input generator (MAZE) [17]. The straight and S-plate wheel models are shown in Figures 3 and 4, respectively.

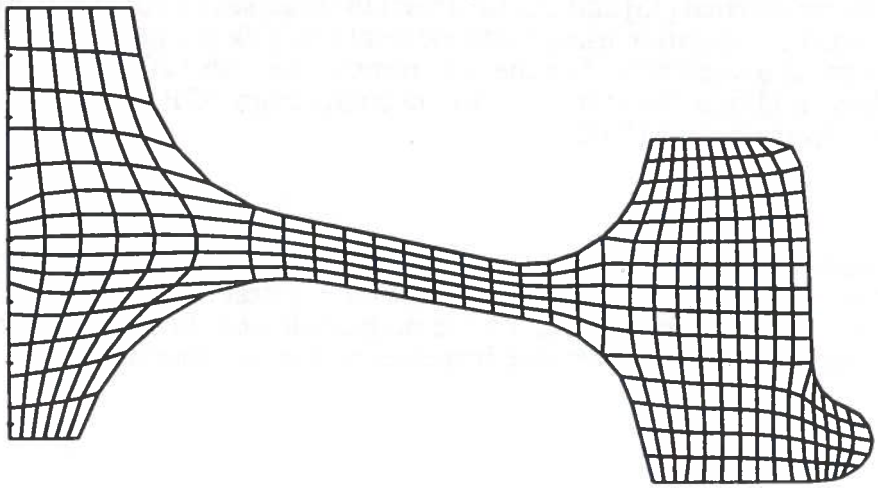

Figure 3. Finite Element Mesh for Straight Plate Wheel.

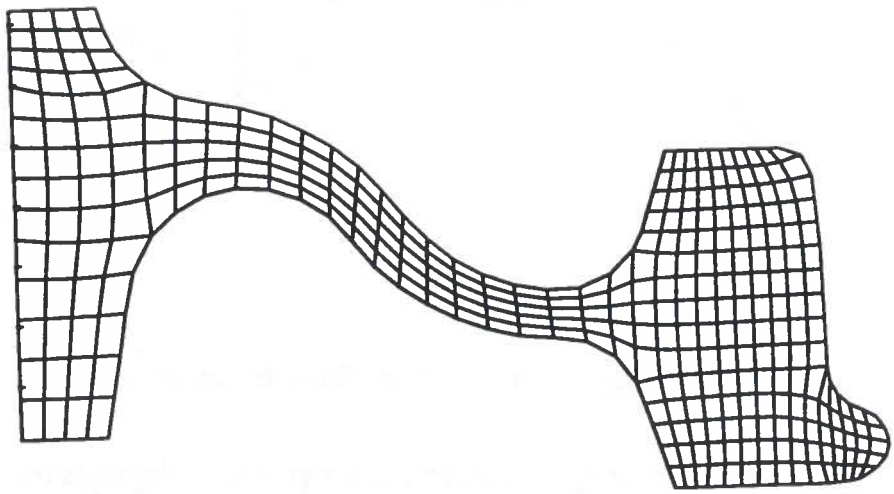

Figure 4. Finite Element Mesh for S-Plate Wheel.

2.2 Material Properties

In the heat transfer analysis (TOPAZ), the material was treated as isotopic with properties independent of temperature. Table 1 summarizes the values assumed.

The thermo-elastic-plastic material model option was used in the stress analysis (NIKE), in order to allow the material mechanical properties to be temperature-dependent. The material property values were taken directly from Lundèn [13] for temperatures between 273 ^{o}K (32 ^{o}F) and 673 ^{o}K (752 ^{o}F). Properties for other temperatures were linearly extrapolated to complete the inputs required by the software. Table 2 summarizes the published and extrapolated values. The yield strength was arbitrarily increased by four orders of magnitude for input to the NIKE software, in order to retain the temperature dependence of the material properties while restricting the calculations to elastic stress analysis.

Table 1. Material Properties Used to Represent Wheel Steel.

Property	Value	Units
Density	7861	kg/m^3
Heat capacity	502.1	J/kg ^{o}K
Thermal conductivity	44.78	W/m ^{o}K

Table 2. Published [13] and Extrapolated Properties for B82 Wheel Steel.

T (^{o}K)	E [a] (GPa)	ν [b]	α [c] (ppm/^{o}K)	σ_Y [d] (MPa)	E_K [e] (GPa)
0	229.1	.2748	9.962	580	15.0
273	210.0	.2830	11.60	570	15.0
373	203.8	.2860	12.20	560	15.0
473	197.5	.2900	12.80	550	15.0
573	191.3	.2940	13.40	540	13.5
673	185.0	.2980	14.00	538	12.0
773	178.7	.3020	14.60	520	10.5
873	172.4	.3060	15.20	510	9.0

[a]Young's modulus [b]Poisson's ratio [c]thermal expansion coefficient
[d]yield strength [e]tangent modulus

2.3 Thermal Loading Conditions

The thermal load due to braking was simulated by applying a uniform heat flux along the tread surface (Figure 5). To simulate heat application through brake shoe, the heat application area was defined as six grid divisions across the tread: a total width of 2.347 inches, which is close to the nominal 2.375-inch brake shoe width. Since train resistance accounts for some of the braking effort and some of the heat is dissipated through the brake shoe, 85% of the total heat flux (as defined by the change in kinetic energy) was applied to the wheel. Average heat flux was computed by converting the initial kinetic energy of the vehicle into an average power input at each wheel, assuming constant deceleration. The instantaneous heat flux thus decreases linearly as a function of time, from an initial value equal to twice the average heat flux.

2.4 Boundary Conditions

To account for the loss of heat through the wheel surfaces, it is important to consider the effect of the surroundings on the wheel during braking operations. Radiation and convection boundary conditions for the wheel are included in the heat transfer analysis. At the surface of the wheel, heat is radiated and convected relative to the ambient temperatures shown in Figure 6. These temperatures represent summer daytime conditions (90 ^{o}F day).

Since the motor is a source of heat, the temperature on the gage side of the wheel is higher than the temperature on the field side. The ambient temperature for heat exchange from the tread surface has an intermediate value as a compromise between the field and gage sides. Calculations for the convection coefficient and the heat transfer coefficient are based on the equations found in the TOPAZ manual [15]. The convection coefficient is computed as:

$$h = 1.31 \Delta T^{1/3} \tag{1}$$

where ΔT is the difference between the wheel surface and ambient temperatures. The heat transfer coefficient is computed as:

$$f = \sigma \epsilon F \tag{2}$$

where σ is the Stefan-Boltzmann constant (5.67×10^{-8} W/m^2^{o}K^4), ϵ is the surface emissivity (0.85 and 0.95 assumed for the tread and faces, respectively), and F is a geometrical view factor (here assumed equal to 1 in all cases).

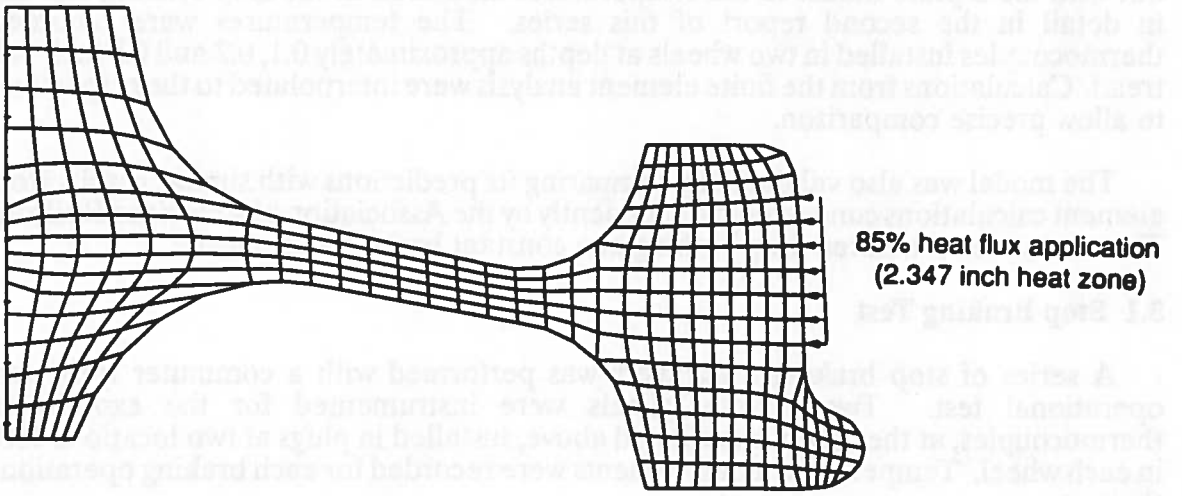

Figure 5. Heat Flux Distribution on the Wheel.

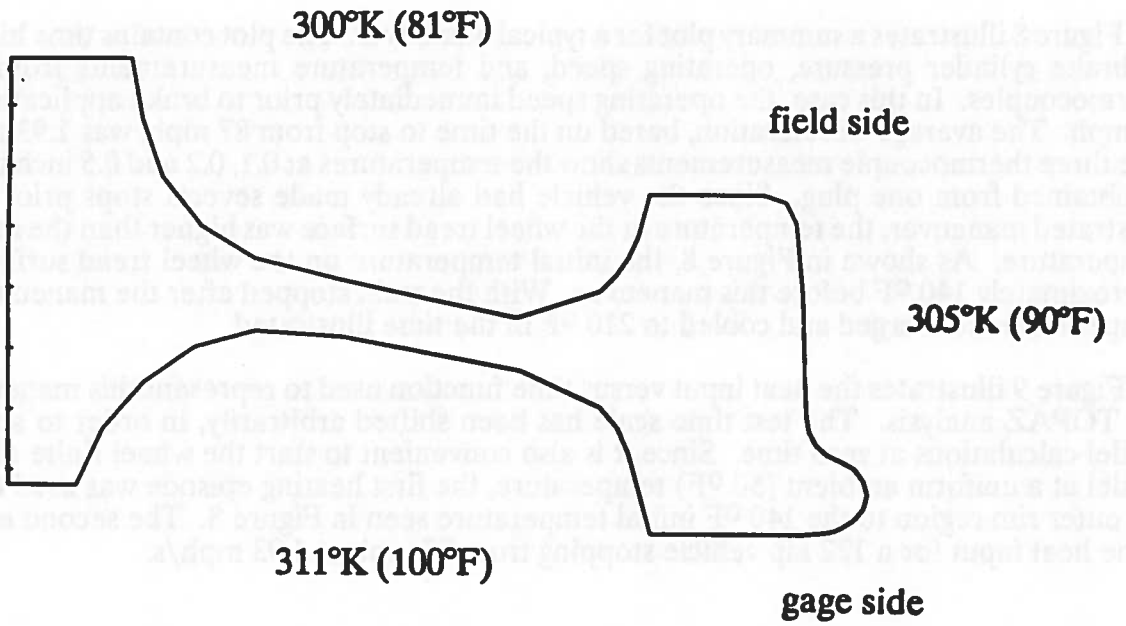

Figure 6. Ambient Temperatures Surrounding the Wheel.

3. MODEL VALIDATION

The models were validated by comparing the transient temperature calculations carried out with the S-plate model to the temperatures measured in the stop braking test discussed in detail in the second report of this series. The temperatures were recorded from thermocouples installed in two wheels at depths approximately 0.1, 0.2 and 0.5 inch below the tread. Calculations from the finite element analysis were interpolated to the respective depths to allow precise comparison.

The model was also validated by comparing its predictions with similar results from finite element calculations conducted independently by the Association of American Railroads [14]. These analyses simulated drag braking at a constant brake horsepower.

3.1 Stop Braking Test

A series of stop braking maneuvers was performed with a commuter train during an operational test. Two S-plate wheels were instrumented for the experiment with thermocouples, at the depths mentioned above, installed in plugs at two locations 180° apart in each wheel. Temperature measurements were recorded for each braking operation during the test.

The speed versus time profiles from several of the braking operations were converted to heat input for finite element analysis. The boundary conditions were based on a 50 °F night (Figure 7) to represent the actual test conditions. The heat input was based on the speed of the vehicle before brake application, the average deceleration, and the actual test vehicle weight of 122 kips.

Figure 8 illustrates a summary plot for a typical maneuver. The plot contains time histories of brake cylinder pressure, operating speed, and temperature measurements from three thermocouples. In this case, the operating speed immediately prior to brake application was 87 mph. The average deceleration, based on the time to stop from 87 mph, was 1.93 mph/s. The three thermocouple measurements show the temperatures at 0.1, 0.2 and 0.5 inch depths, as obtained from one plug. Since the vehicle had already made several stops prior to the illustrated maneuver, the temperature at the wheel tread surface was higher than the ambient temperature. As shown in Figure 8, the initial temperature on the wheel tread surface was approximately 140 °F before this maneuver. With the train stopped after the maneuver, the temperatures converged and cooled to 210 °F in the time illustrated.

Figure 9 illustrates the heat input versus time function used to represent this maneuver in the TOPAZ analysis. The test time scale has been shifted arbitrarily, in order to start the model calculations at zero time. Since it is also convenient to start the wheel finite element model at a uniform ambient (50 °F) temperature, the first heating episode was used to heat the outer rim region to the 140 °F initial temperature seen in Figure 8. The second episode is the heat input for a 122 kip vehicle stopping from 87 mph at 1.93 mph/s.

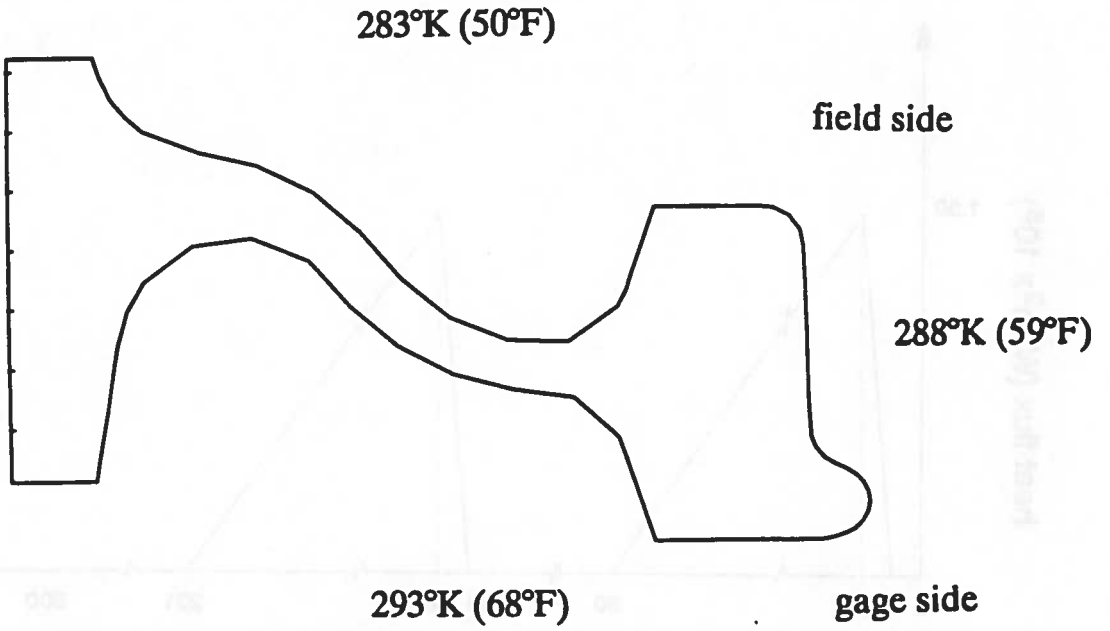

Figure 7. Ambient Temperatures for the Stop Braking Test.

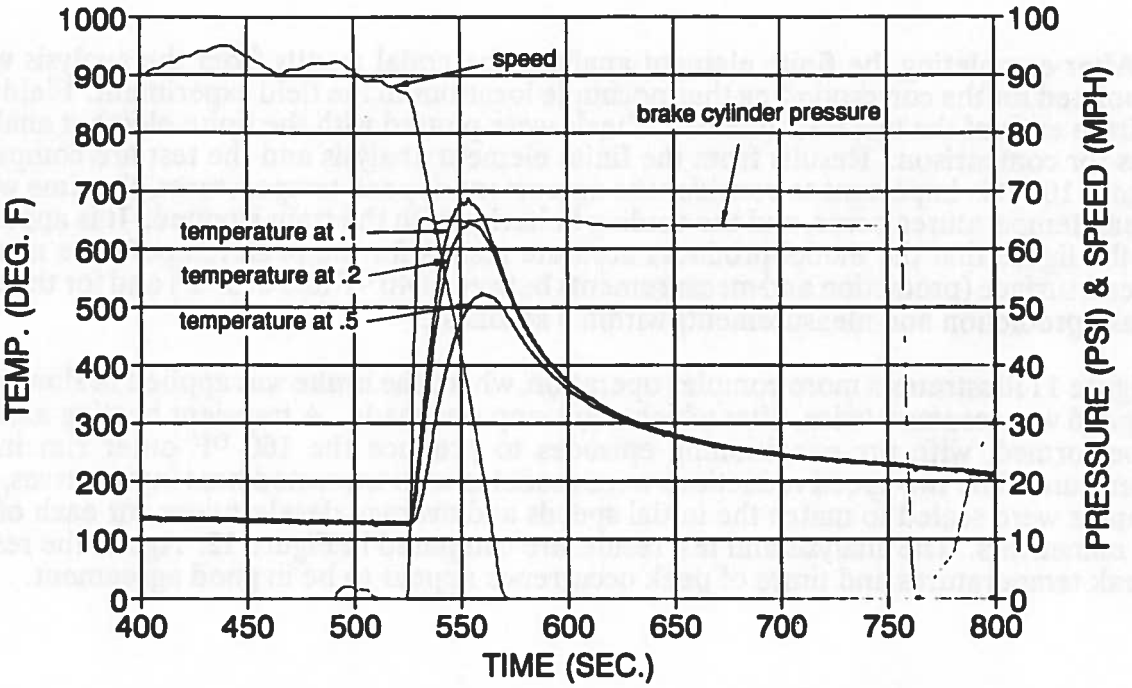

Figure 8. Summary Plot for One Full Service Braking Maneuver.
(Initial speed = 87 mph, average deceleration = 1.93 mph/s.)

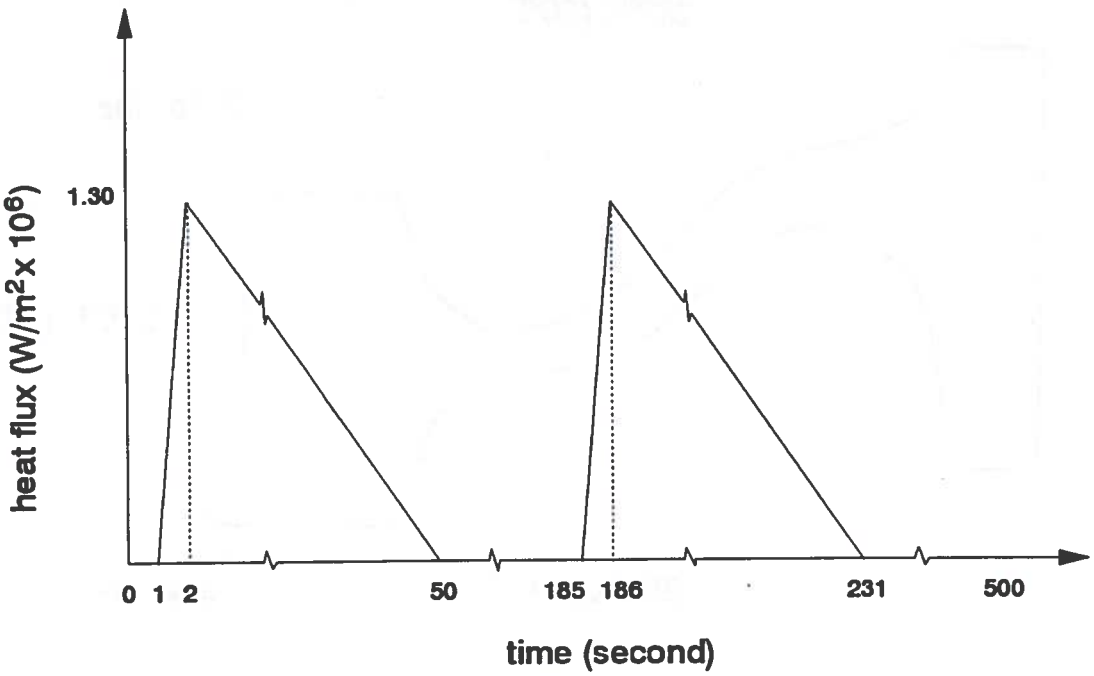

Figure 9. Heat Input to Represent the Maneuver Shown in Figure 8.

After completing the finite element analysis, the nodal results from the analysis were interpolated for the corresponding thermocouple locations in the field experiment. Field test data from each of the two instrumented wheels were plotted with the finite element analysis results for comparison. Results from the finite element analysis and the test are compared in Figure 10. It is important to consider the agreement of peak temperatures, the time when the peak temperatures occur, and the cooling behavior with the train stopped. It is apparent from the figure that the model produces accurate results for the peak temperature nearest the tread surface (prediction and measurements between 640 ^{o}F and 675 ^{o}F) and for the time to peak (prediction and measurements within 5 seconds).

Figure 11 illustrates a more complex operation, where the brake was applied to slow down and speed was resumed twice, after which a full stop was made. A transient heating analysis was performed, with pre-conditioning episodes to produce the 160 ^{o}F outer rim initial temperature. The two speed reductions were modeled with truncated heat input curves, and the inputs were scaled to match the initial speeds and average decelerations for each of the three maneuvers. The analysis and test results are compared in Figure 12. Again, the results for peak temperatures and times of peak occurrence appear to be in good agreement.

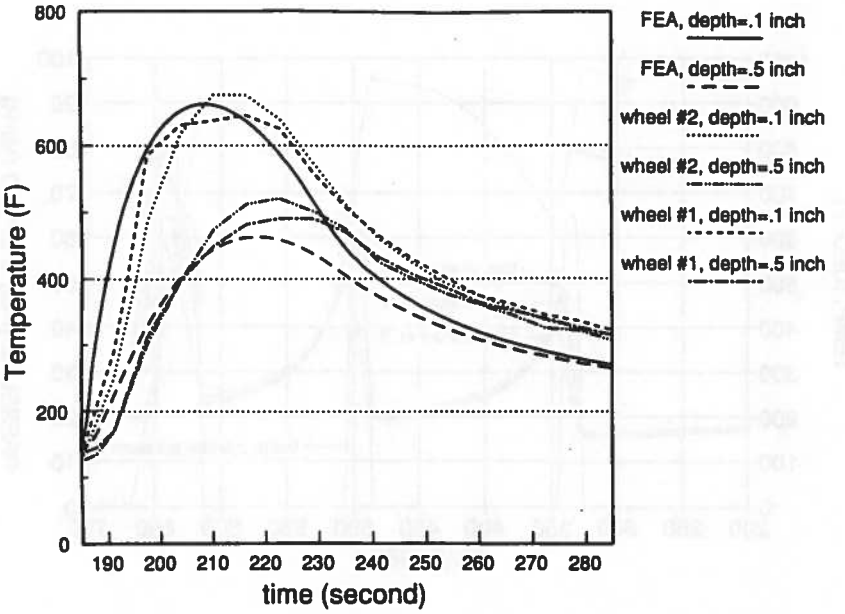

Figure 10. Comparison of Calculated and Measured Temperatures.
(Full service stop from 87 mph at 1.93 mph/s.)

Several other single, full service braking maneuvers were also compared. These comparisons show variations of measured temperatures, with the finite element analysis results tending to predict the average behavior (see Appendix A). The measured temperature variations are believed to have resulted from variations of the brake shoe friction coefficient.

There is less agreement between the predictions and results for cooling behavior, the model tending to exhibit somewhat quicker cooling than indicated by the measurements. The difference is believed to result from the simplified assumption that only 85% of the vehicle energy is dissipated into the wheel (see Section 2.3). In reality, the 15% deduction covers both other heat sinks (brake shoes and rail) and train resistance. Based on accepted empirical factors [18], the effect of train resistance for the test conditions is estimated to account for about 9% of the energy dissipation at typical initial speeds, but the proportion declines to about 7% at 70 mph and 5% at 50 mph.

Although the model over-estimates the effect of train resistance at lower speeds, it is well suited to the first part of a stop braking maneuver, when temperatures peak in the outer rim region. Overall, there is no significant difference between the calculations and the test results.

3.2 Drag Braking Analysis

The Association of American Railroads (AAR) has developed a well established finite element analysis procedure for evaluating the ability of a wheel to tolerate drag braking (a condition expected in freight service, where the air brakes must be used to balance heavy

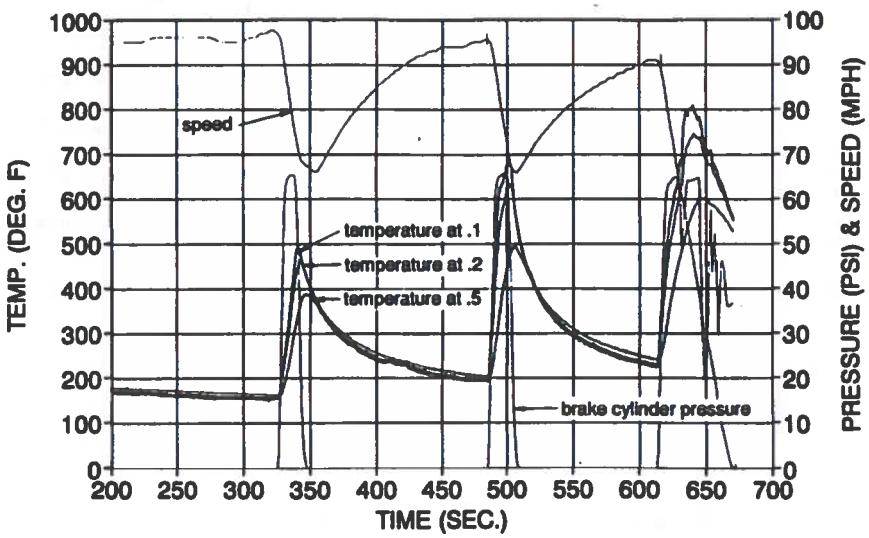

Figure 11. Summary Plot for a Complex Operation.

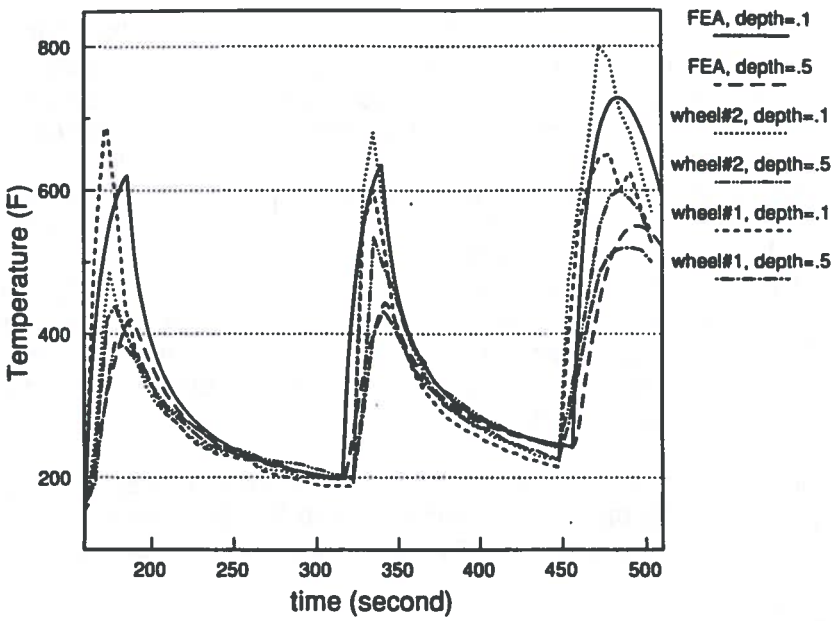

Figure 12. Comparison of Calculated and Measured Temperatures.

trains at constant speed on long down grades). A similar condition may happen occasionally in passenger service, when minor malfunctions in the magnet valve portion of the electropneumatic passenger brake systems prevent complete release. Drag braking in either situation usually involves relatively small fluctuations of input brake horsepower about an average value. The average brake horsepower is generally much lower than the initial instantaneous values associated with stop braking from high speeds. However, the drag braking horsepower may be applied to the wheel continuously for 20 minutes or more.

The AAR conducted drag braking analyses of the 32-inch commuter car wheel to compare a flexible S-plate design with the original straight plate wheel [14]. The conditions used for the analyses were continuous application of 29.28 BHp for 20 minutes.

Similar analyses were conducted with the present model in order to compare its results with those obtained by the AAR. The only change made was the heat input curve: a linear ramp to 1.21×10^5 W/m^2, followed by continuous application until 20 minutes elapsed. (When multiplied by the brake shoe width and wheel circumference, the heat flux value corresponds to 85% of 29.28 BHp.)

Figure 13 compares temperature contour plots from the two straight plate wheel models at the end of the drag braking period. Figure 14 illustrates a comparison of the corresponding elastic thermal stresses. Overall, there is no significant difference between the two results. Similar agreement was observed in the analyses of the S-plate design.

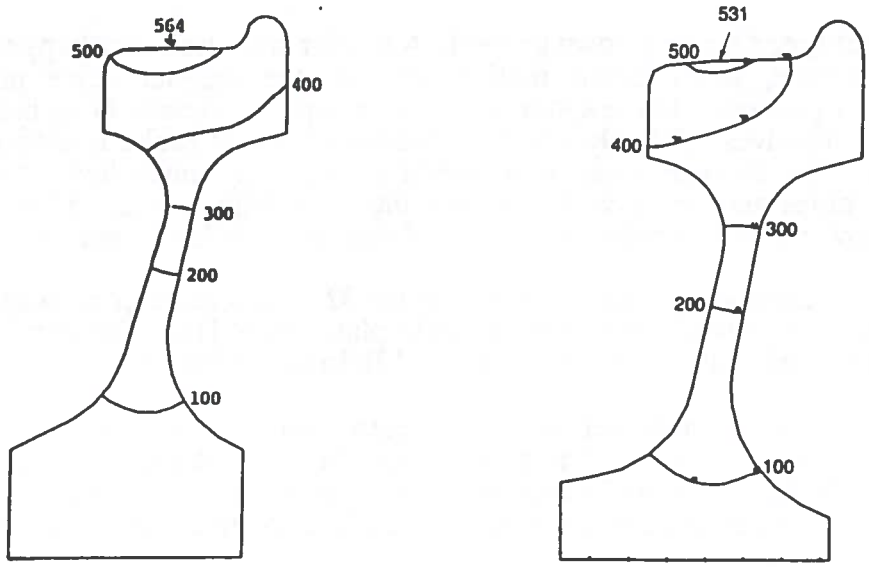

Figure 13. Temperature Distributions Calculated for Drag Braking. (Contour interval 100 °F.)

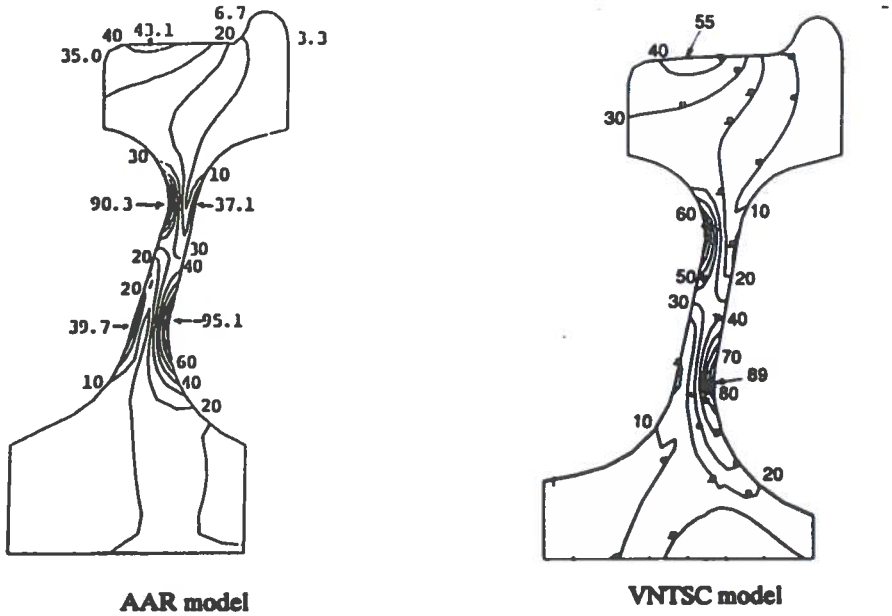

Figure 14. Effective Stress Distributions Calculated for Drag Braking. (Contour interval 10 ksi; 1 ksi = 6.9 MPa.)

4. SENSITIVITY STUDY

The validated model was used to study the effects of operating speed, average deceleration, and wheel plate design on the temperature and stress distributions in wheels subjected to stop braking. Table 3 summarizes the operating scenarios and thermal inputs.

Table 3. Stop Braking Cases Analyzed for Sensitivity Study.

Initial Speed (mph)	Avg. Deceleration (mph/sec)	Stop Time (sec)	Maximum Flux (MW/m^2)
80	2	40.0	1.424
80	3	26.7	2.136
100	2	50.0	1.780

Computations for the heat transfer analysis were made for a period of 100 seconds at one second intervals. Peak temperatures and temperature gradients were identified by means of temperature-time history plots. Figure 15 illustrates a temperature-time history plot for a straight plate wheel during a stop from 100 mph at 2 mph/s. The three curves correspond to the three nodes located nearest to the center of the tread surface (Figure 16). As shown in Figure 15, the tread surface temperature increases to its maximum at 22 seconds after brake application. Note that the temperatures below the surface reach their maxima at slightly later times, but that in each case, cooling starts before the car has come to a standstill. By 100 seconds, the outer rim is cooling slowly, and the temperature gradient has almost disappeared. Figure 17 shows the temperature distribution in the wheel at the time its tread surface temperature peaks. The contours illustrate the high gradient of temperature near the tread surface. This result is typical for stop braking (contrast this plot with the distributions shown in Figure 13).

Appendices B and C contain the complete set of temperature-time history and contour plots for the sensitivity study. These results show that the peak tread temperature is attained at 14 to 22 seconds after brake application, for the cases considered, and that the plate design (straight or S) has no significant effect on the response.

Elastic thermal stresses were computed for the same 100-second period at one-second intervals. The computed states were inspected for a small range of times at which the largest temperature gradients appeared in the transient heating analysis. The state of maximum stress was approximated by the computed state with the greatest stress. Figure 18 illustrates the effective stress[9] distribution obtained for the preceding example. The computed values exceed the material yield strength because the elastic analysis does not account for yielding. The elastic stress is thus not a direct indicator of what can actually happen to the wheel, but the result is useful for comparison of different cases. Appendix D contains the complete set of contour plots for the sensitivity study.

---

9 Effective stress is also referred to as Mises-Hencky equivalent stress or octahedral shear stress.

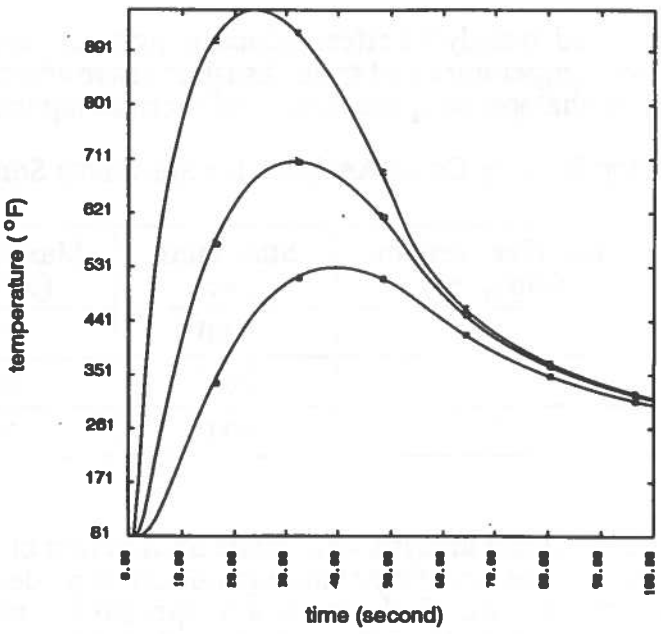

Figure 15. Outer Rim Temperatures During Stop from 100 mph at 2 mph/s.

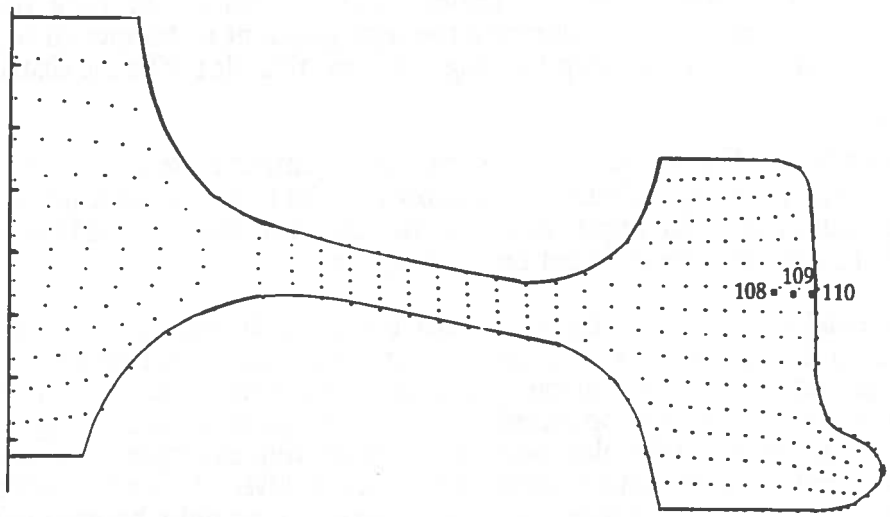

Figure 16. Locations of Temperatures Plotted in Figure 15.

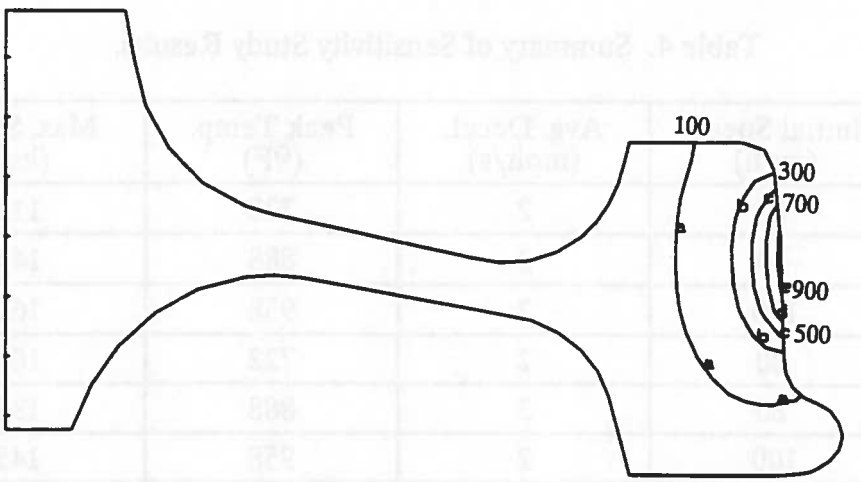

Figure 17. Temperature Distribution for Case Shown in Figure 15.
(Temperatures at 22 sec after brake application; contour interval 200 ^{o}F.)

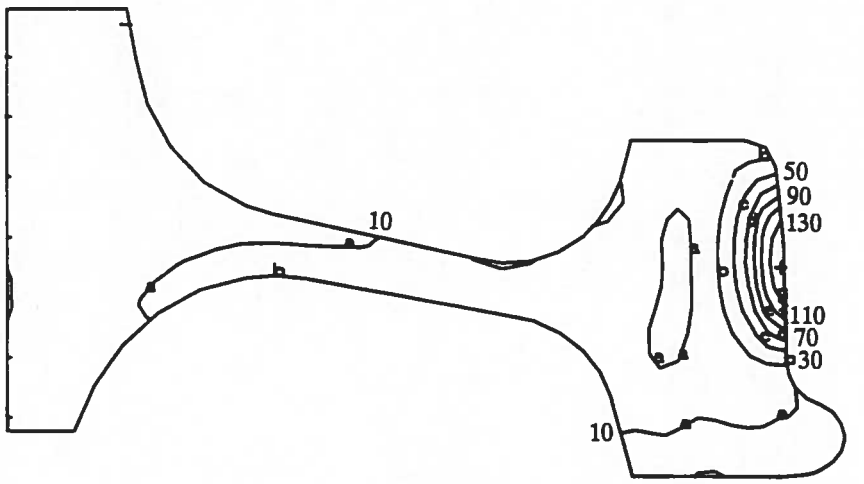

Figure 18. Effective Stress Distribution for Case Shown in Figure 15.
(Stress at 22 sec after brake application; contour interval 20 ksi; 1 ksi = 6.9 MPa.)

Table 4 summarizes the study results. Both initial speed and deceleration rate have a significant effect on the peak tread surface temperature and the maximum effective stress. Contrary to what has been found for drag braking, however, the S plate flexibility has only a small effect on reduction of the thermal stress.

Table 4. Summary of Sensitivity Study Results.

Plate design	Initial Speed (mph)	Avg. Decel. (mph/s)	Peak Temp. (^{o}F)	Max. Stress (ksi)
Straight	80	2	723	112
	80	3	888	141
	100	2	958	160
S	80	2	722	109
	80	3	888	138
	100	2	958	145

5. DISCUSSION AND CONCLUSIONS

The present models of the 32-inch diameter, reversed dish, straight and S plate wheels are well calibrated for the intended purpose, namely, study of the effects of stop braking from operating speeds in the 80 to 100 mph range. Similar models of other size brake shoes or wheels would be equally useful for other services where the effects of stop braking on wheel performance might be of concern.

Re-calibration may be required for analyses of other speed regimes or other wheel sizes. Deducting 15% of the heat input, as is done in the present model, actually represents train resistance and other heat sinks which account for roughly 10% and 5%, respectively, in the 80 to 100 mph speed regime. For other speeds, one should at least use the Davis equation [18] to re-estimate the train resistance deduction. For brake shoes or wheels of other sizes, some adjustment of the heat sink deduction may be necessary.

The stop braking cases presented in this report approximate the operations on existing commuter lines served by electric MU cars. The study results leave no doubt that such operations can produce excessively high temperatures on the wheel tread surface unless auxiliary brakes are available to absorb some of the vehicle kinetic energy.

Stop braking also causes large thermal stresses when the wheel temperature distribution is nonuniform. The stress effects due to stop braking are qualitatively and quantitatively different from those due to drag braking. The highest effective stresses from stop braking are found near the tread surface, whereas in drag braking they occur near the plate fillet areas. The effective stresses calculated for stop braking are 20 to 50% larger than the stresses calculated for drag braking of a straight plate wheel. Also, whereas the flexible plate is able to reduce drag braking stress by 30 to 50%, the reduction of stop braking stress is less than 10%, even though a typical stop braking event imposes only 20% of the total heat energy dissipated during the representative drag braking scenario.

Seasonal variation of ambient temperature may have some effect on wheel performance. Winter conditions may lead to larger temperature gradients and, consequently, larger thermal stresses during stop braking. However, the wheel plate soaks quickly to temperatures in the 150 to 250 ^{o}F regime when repeated stops are made. Therefore, any winter effect may be confined to the first stop in a run.

The concentration of heat evident in the stop braking analyses suggests that brake shoe width is a parameter deserving study. A wider shoe might provide some relief from the severity of stop braking. Quantitative assessment of other conditions, such an overhanging shoes, could also be included in such a study.

REPORTS IN THIS SERIES

1. O. Orringer, D.E. Gray, and R.J. McCown, "Evaluation of immediate actions taken to deal with cracking problems observed in wheels of rail commuter cars," Volpe National Transportation Systems Center, Cambridge, MA, and Federal Railroad Administration, Washington, DC, report no. FRA/ORD-93/15, July 1993.
2. C. Stuart and S. Yu, "Thermal measurements of commuter rail wheels under revenue service conditions," Ensco, Inc., Springfield, VA, report no. FRA/ORD-93/19, September 1993.

REFERENCES

[1] S. Yu and C. Stuart, "Wheel peeling experiment report for the cracked wheel investigation," Ensco, Inc., Springfield, VA, May 1992.

[2] C. Stuart and R.J. McCown, "Wheel saw-cutting experiment report for the cracked wheel investigation," Ensco, Inc., Springfield, VA, May 1992.

[3] M.R. Johnson, R.R. Robinson, A.J. Opinsky, M.W. Joerms, and D.H. Stone, "Calculation of residual stresses in wheels from saw cut displacement data," American Society of Mechanical Engineers, New York, paper no. 85-WA/RT-17, November 1985.

[4] R.M. Pelloux and J. Liang, "Metallographic examination of thermally cracked commuter car wheels," Department of Materials Science and Engineering, MIT, July 1992.

[5] P. Clayton, "Hot compression tests on the Gleeble 1500," Oregon Graduate Institute of Science & Technology, Beaverton, OR, November 1992.

[6] R.M. Pelloux and J. Liang, "Hot compression tests and metallographic examination of Class L rail wheel alloy," Department of Materials Science and Engineering, MIT, December 1992.

[7] J. Orkisz, O. Orringer, M. Holowinski, M. Pazdanowski, and W. Cecot, "Discrete analysis of actual residual stresses resulting from cyclic loadings," *Computers & Structures 35(4)*, 397-412 (1990).

[8] O. Orringer, J. Orkisz, and Z. Swiderski (ed.), *Residual Stress in Rails: Effects on Rail Integrity and Railroad Economics*, Kluwer Academic Publishers, Boston, 1992.

[9] J. Orkisz and M. Holowinski, "Prediction of residual stresses in rails: practical benefits from theoretical approach," *Proc. FRA/ERRI International Conference on Rail Quality and Maintenance for Modern Railway Operation*, Delft, The Netherlands, June 1992 (in press).

[10] A.B. Perlman, J.E. Gordon, and O. Orringer, "Effect of grinding strategy on residual stress in the rail head," *Proc. FRA/ERRI International Conference on Rail Quality and Maintenance for Modern Railway Operation*, Delft, The Netherlands, June 1992 (in press).

[11] K.L. Johnson, *Contact Mechanics*, Cambridge University Press, Cambridge, England, 1985.

[12] A. Martin Meizoso, J.M. Martinez Esnaola, and M. Fuentes Pèrez, "Approximate crack growth estimate of railway wheel influenced by normal and shear action," *Theoretical and Applied Fracture Mechanics 15*, 179-190 (1991).

[13] R. Lundèn, "Contact region fatigue of railway wheels under combined mechanical rolling pressure and thermal brake loading," *Wear 144*, 57-70 (1991).

[14] A.J. Opinsky and M.W. Joerms, "Finite element stress analysis of three Edgewater 32 inch wheel designs," Association of American Railroads, Chicago Technical Center, Chicago, IL, report no. LT-638, March 1986.

[15] A.B. Shapiro, "TOPAZ2D - A two-dimensional finite element code for heat transfer analysis, electrostatics, and magnetostatics problems," Lawrence Livermore National Laboratory, Livermore, CA, UCID-20824, July 1986.

[16] B. Engelmann and J.O. Hallquist, "NIKE2D - A nonlinear, implicit, two-dimensional finite element code for solid mechanics," Lawrence Livermore National Laboratory, Livermore, CA, UCRL-MA-105413, April 1991.

[17] J.O. Hallquist, "MAZE - An input generator for DYNA2D and NIKE2D," Lawrence Livermore National Laboratory, Livermore, CA, UCID-19029 Rev. 2, June 1983.

[18] H.H. Jones et al., *Engineering and Design of Railway Brake Systems*, Air Brake Association, Chicago, IL, September 1975.

APPENDIX A

COMPARISONS OF FINITE ELEMENT MODEL CALCULATIONS WITH TEMPERATURE MEASUREMENTS FROM STOP BRAKING TEST

Table A.1 Summary of Cases.

Figure	Initial Speed (mph)	Avg. Decel. (mph/s)
10	87	1.93
A.1	94	1.61
A.2	91	1.82
A.3	90	1.70
A.4	99	1.68

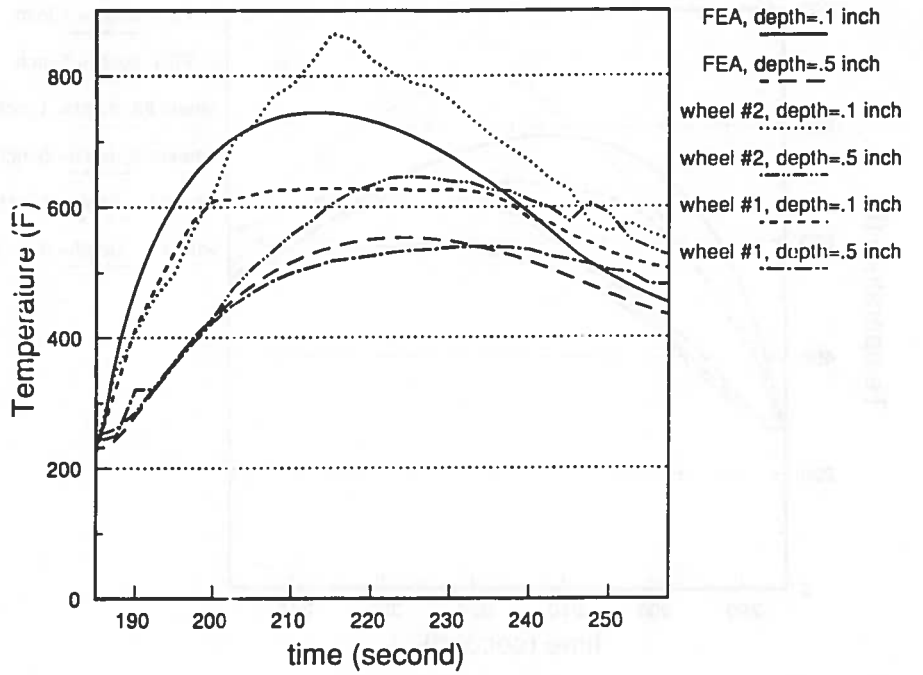

Figure A.1

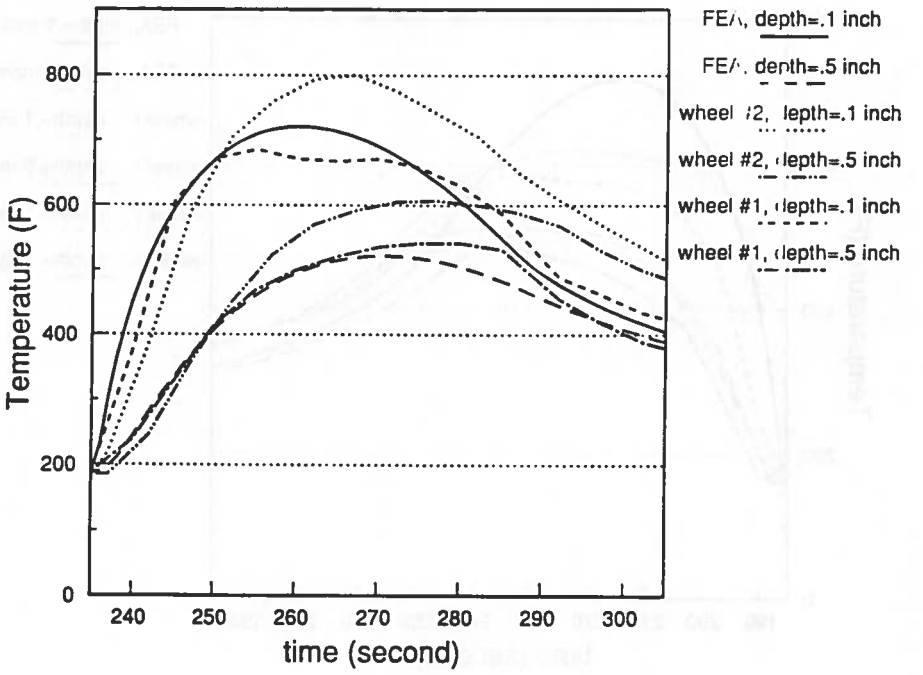

Figure A.2

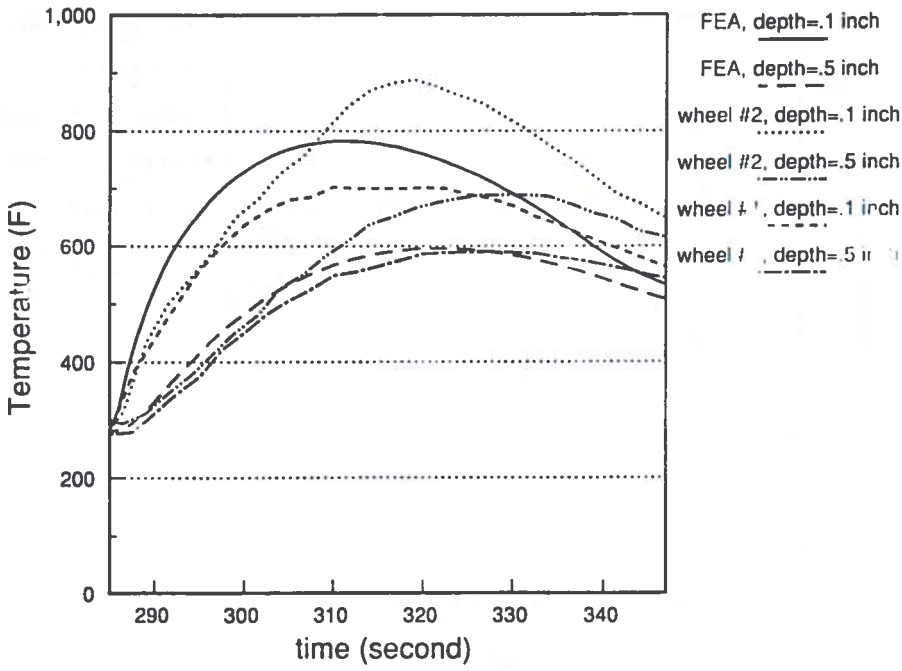

Figure A.3

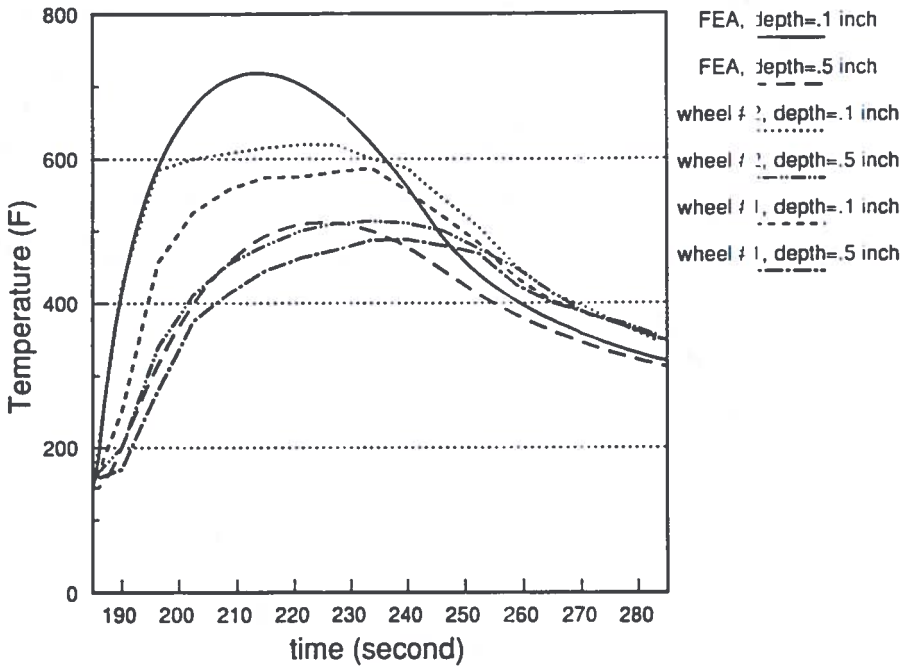

Figure A.4

APPENDIX B

OUTER RIM TRANSIENT TEMPERATURES CALCULATED FOR STOP BRAKING SENSITIVITY STUDY

Table B.1. Summary of Cases

Figure	Initial Speed (mph)	Avg. Decel. (mph/s)	Plate Design
B.1	80	2	straight
B.2	80	3	straight
15	100	2	straight
B.3	80	2	S
B.4	80	3	S
B.5	100	2	S

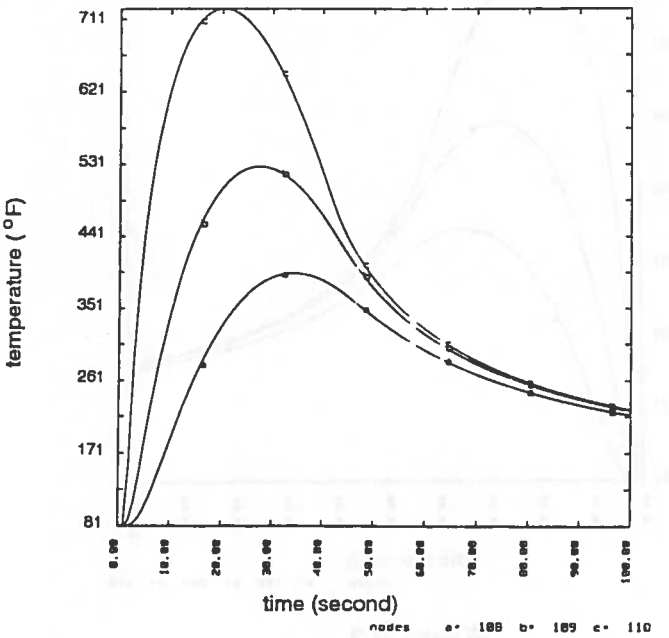

Figure B.1

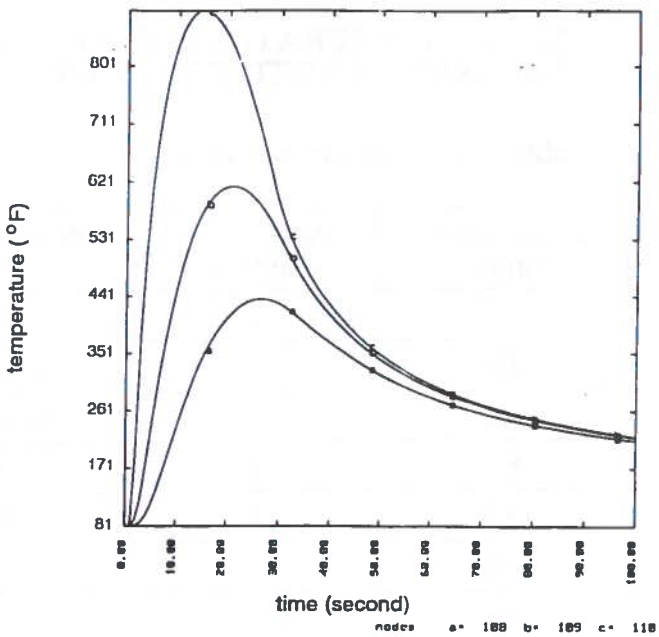

Figure B.2

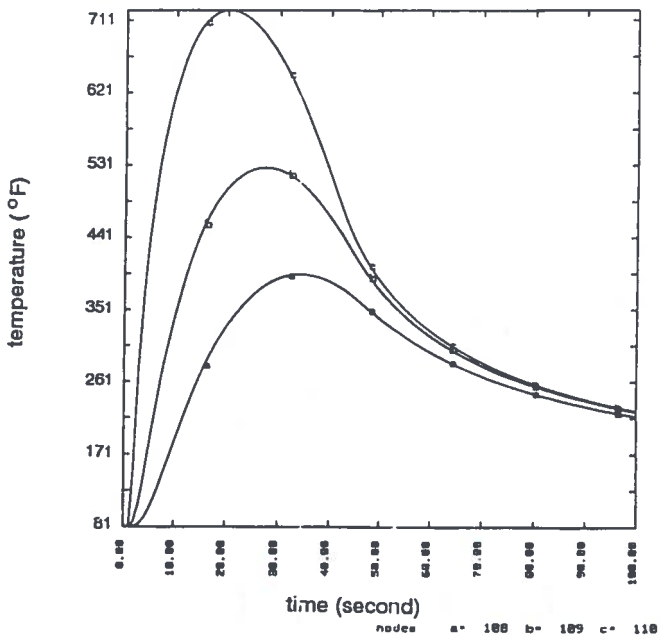

Figure B.3

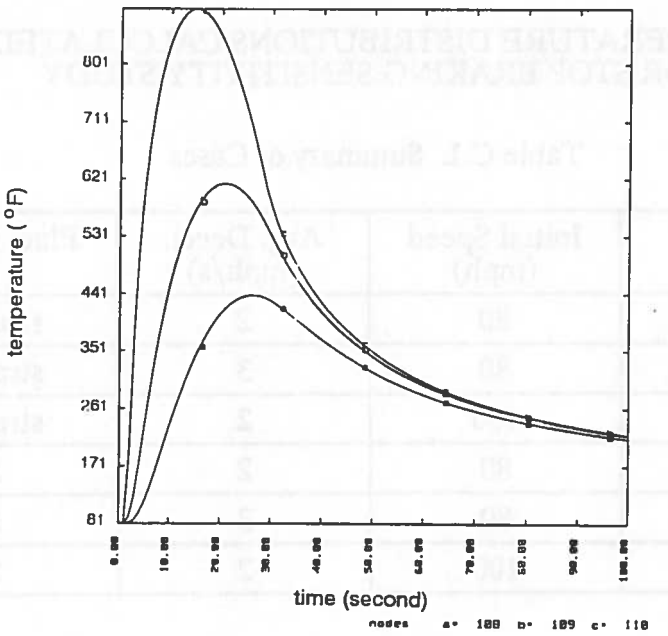

Figure B.4

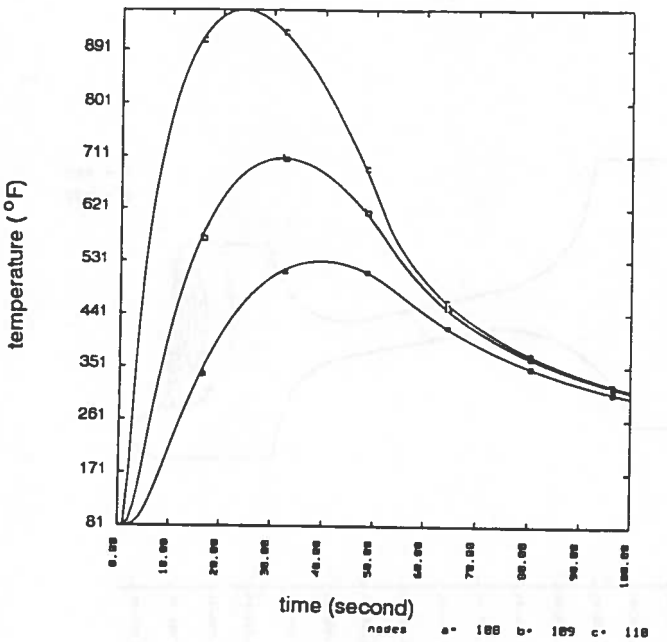

Figure B.5

APPENDIX C

TEMPERATURE DISTRIBUTIONS CALCULATED FOR STOP BRAKING SENSITIVITY STUDY

Table C.1. Summary of Cases

Figure	Initial Speed (mph)	Avg. Decel. (mph/s)	Plate Design
C.1	80	2	straight
C.2	80	3	straight
17	100	2	straight
C.3	80	2	S
C.4	80	3	S
C.5	100	2	S

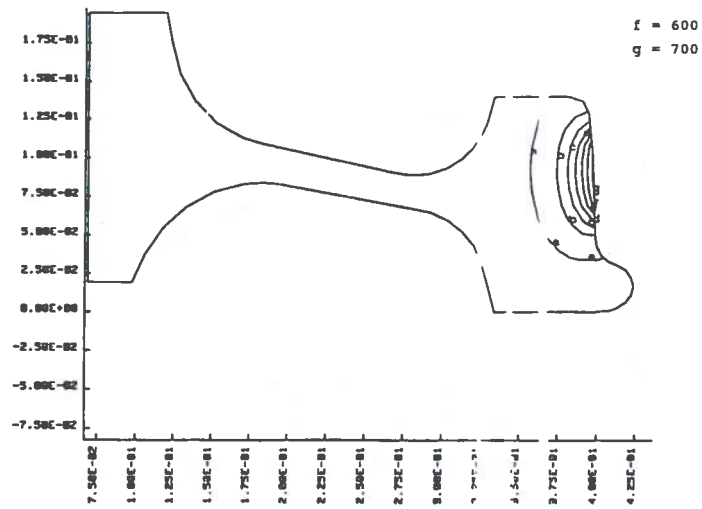

Figure C.1

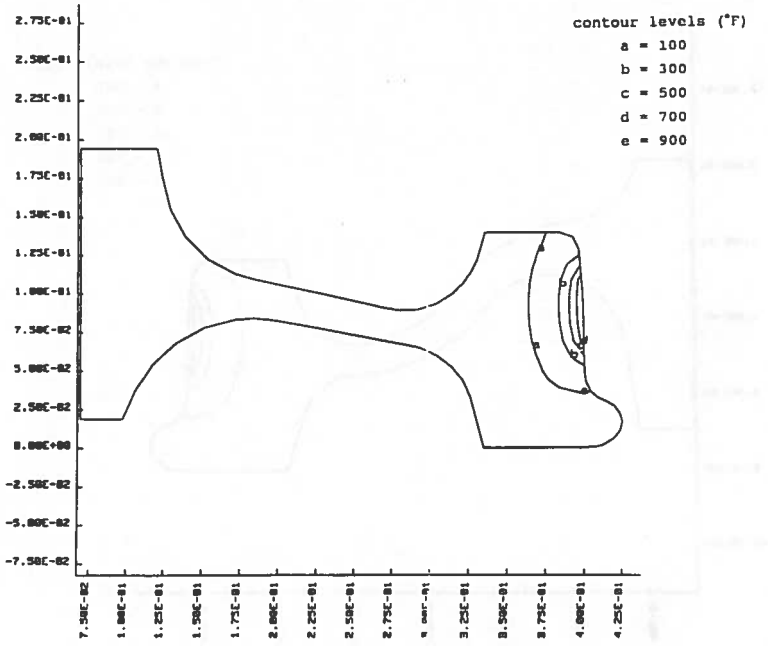

Figure C.2

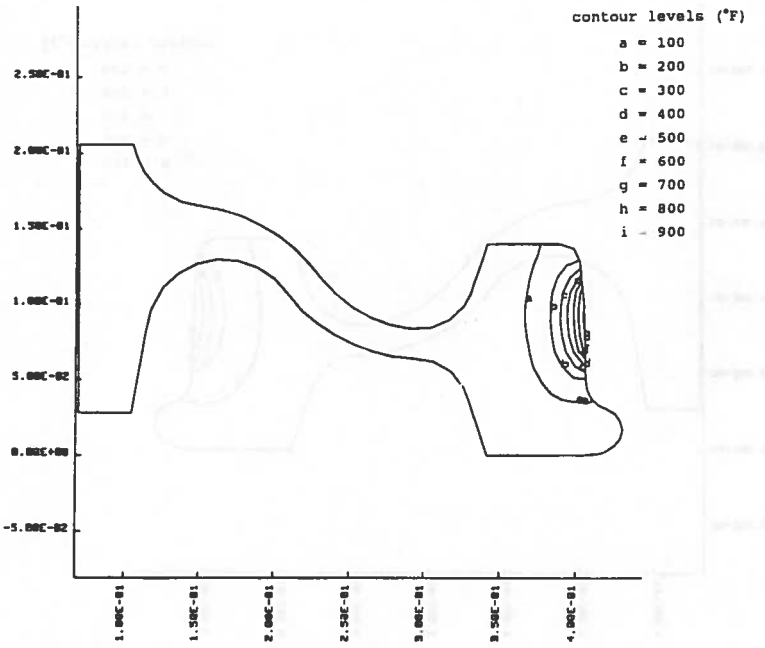

Figure C.3

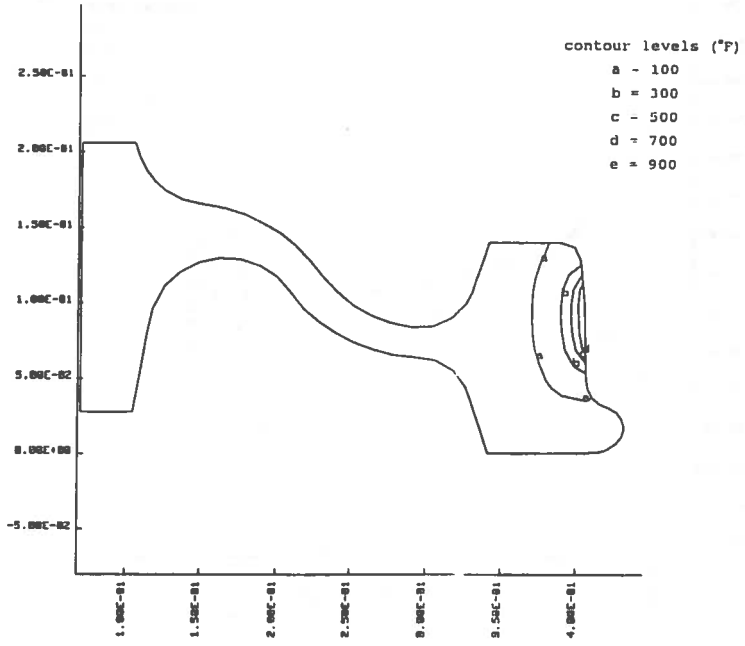

Figure C.4

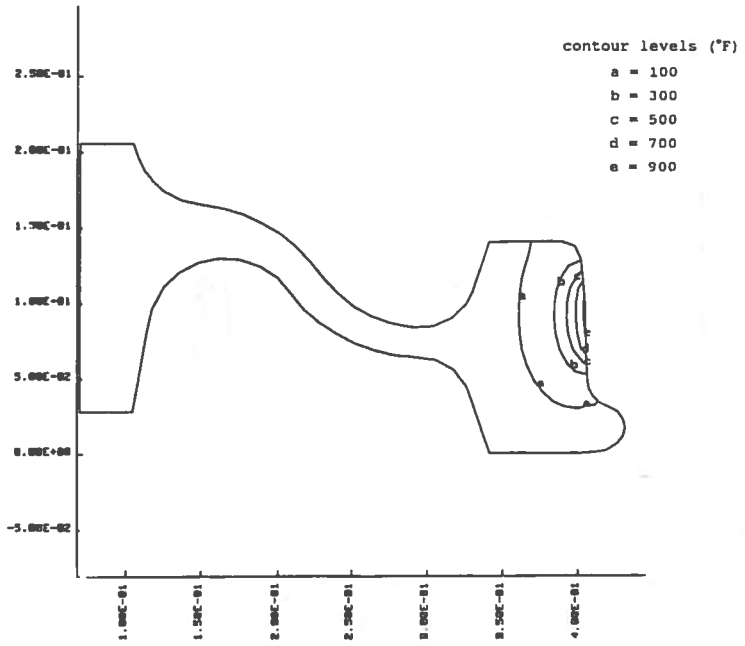

Figure C.5

APPENDIX D

EFFECTIVE ELASTIC THERMAL STRESS DISTRIBUTIONS CALCULATED FOR STOP BRAKING SENSITIVITY STUDY

Table D.1. Summary of Cases

Figure	Initial Speed (mph)	Avg. Decel. (mph/s)	Plate Design
D.1	80	2	straight
D.2	80	3	straight
18	100	2	straight
D.3	80	2	S
D.4	80	3	S
D.5	100	2	S

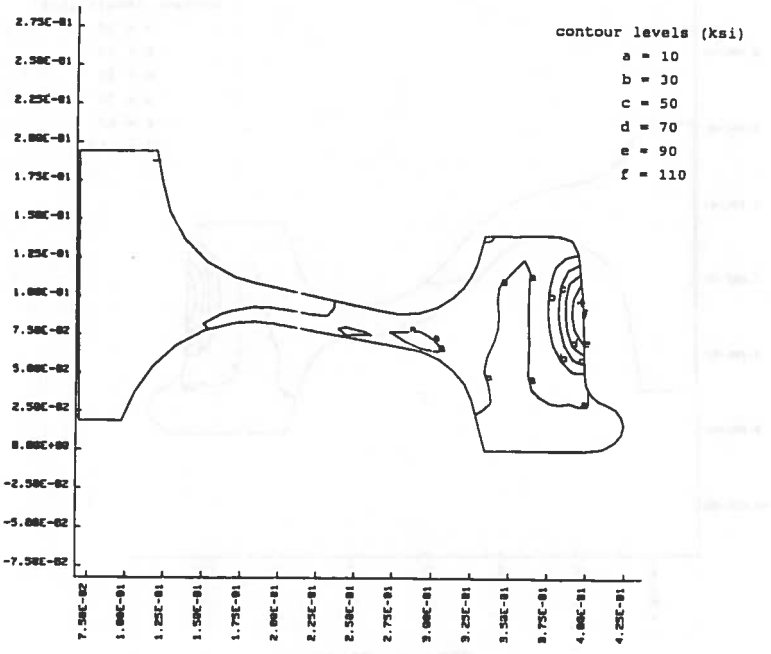

Figure D.1

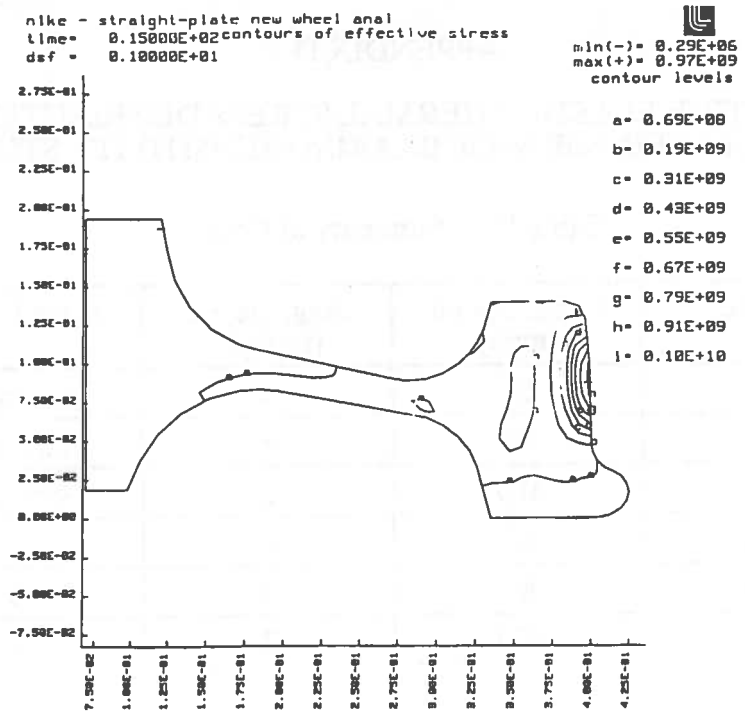

Figure D.2

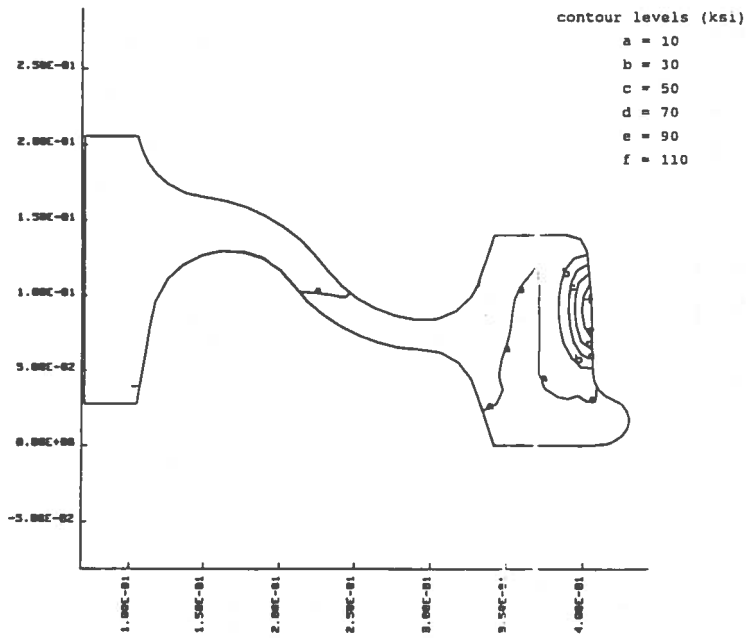

Figure D.3

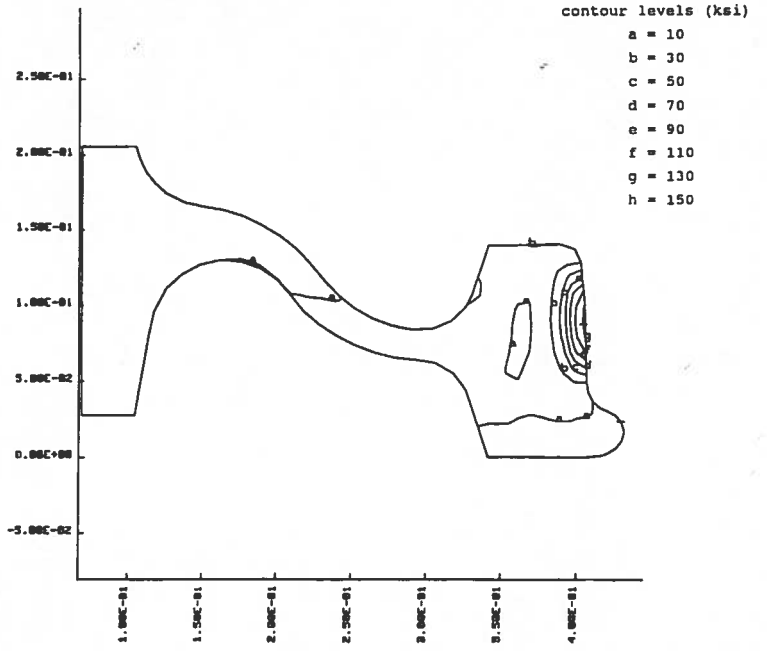

Figure D.4

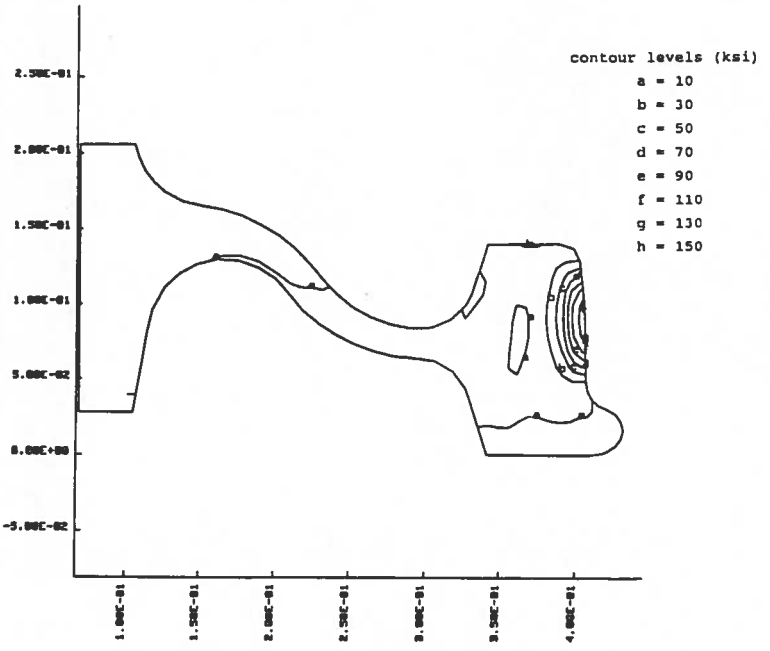

Figure D.5